Structural, magnetic and electrical properties of $SrRuO_3$ films and $SrRuO_3/SrTiO_3$ superlattices

2013 J. Phys.: Condens. Matter 25 496003

(http://iopscience.iop.org/0953-8984/25/49/496003)

IOP PUBLISHING JOURNAL OF PHYSICS: CONDENSED MATTER

J. Phys.: Condens. Matter **25** (2013) 496003 (11pp) doi:10.1088/0953-8984/25/49/496003

Structural, magnetic and electrical properties of $SrRuO_3$ films and $SrRuO_3/SrTiO_3$ superlattices

F Bern[1], M Ziese[1], A Setzer[1], E Pippel[2], D Hesse[2] and I Vrejoiu[2,3]

[1] Division of Superconductivity and Magnetism, Faculty of Physics and Geosciences, University of Leipzig, D-04103 Leipzig, Germany
[2] Max Planck Institute of Microstructure Physics, D-06120 Halle, Germany

E-mail: ziese@physik.uni-leipzig.de

Received 3 September 2013, in final form 30 September 2013
Published 1 November 2013
Online at stacks.iop.org/JPhysCM/25/496003

Abstract

$SrRuO_3$ films and $SrRuO_3/SrTiO_3$ superlattices grown on $SrTiO_3$(001) were studied by structural, magnetic, magnetoresistance and Hall effect measurements. The superlattices showed heteroepitaxial growth with coherent interfaces and a Ru/Ti diffusion region of 1–1.5 unit cells. The resistivity had metallic character above a critical thickness of 3–4 unit cells, becoming insulating below. There was no hint of conduction processes along the interfaces. Both magnetization and magnetoresistance measurements showed an increase of the magnetic anisotropy, consistent with magnetostriction effects. The magnetostriction coefficient was estimated as $\lambda_{100} \sim 1.4 \times 10^{-4}$. Three unit cell thick $SrRuO_3$ layers in $SrRuO_3/SrTiO_3$ superlattices were found to have tetragonal crystal symmetry, as deduced from the sign change of the anomalous Hall constant.

(Some figures may appear in colour only in the online journal)

1. Introduction

At the interface between two complex oxides charge carriers may be confined leading to the emergence of strong correlation and collective effects. In the system $SrTiO_3/LaAlO_3$ superconducting [1] and ferromagnetic [2] phases were observed and even the coexistence of these two phases was reported [3–6]. The mechanism leading to ferromagnetism in this 2D system [7, 8] has not yet been clarified. From an experimental point of view, there is an ongoing debate as to whether the $SrTiO_3/LaAlO_3$ interface is a valid model system for the test of fundamental theories, since the interface between the constituents is not sharp, and might be affected by intermixing [9]. Looking for other oxide systems, the occurrence of a highly confined, two-dimensional electron gas at the $SrTiO_3/SrRuO_3$ interface was theoretically predicted [10, 11]. This is of high interest, because this electron gas was predicted to be half-metallic, inheriting its ferromagnetic order from the 4d states of the Ru^{4+} ions. A verification of this prediction and an analysis of electronic data would have the potential to clarify the role of the 4d-derived Ru bands and the 3d-derived Ti bands in the magnetic order of these systems. First experimental evidence has indicated the presence of a ferromagnetic state in $SrRuO_3/SrTiO_3$ superlattices with a layer thickness of one unit cell [12]. This is surprising, since data on ultrathin $SrRuO_3$ films grown on $SrTiO_3$ showed a strong suppression of the magnetic moment below a layer thickness of 4 ML and indications of the appearance of an interfacial antiferromagnetic layer [13]. The reason underlying this reconstructed ferromagnetic order is not clear at present. It might be due to a suppressed magnetic moment at the interfacial Ru site, but also due to an induced magnetic moment on the Ti site that interacts with the Ru moment via the exchange interaction along the Ru–O–Ti bond. Indeed, studies of the $SrRuO_3/SrMnO_3$ interface showed a related effect, namely the presence of exchange biasing [14, 15]

[3] Present address: Max Planck Institute for Solid State Research, D-70569 Stuttgart, Germany.

Table 1. Layer thicknesses from HRTEM (in unit cells, uc), bilayer thickness t_B (in uc) from x-ray, average lattice constant a, $SrRuO_3$ Curie temperatures T_C, saturation magnetic moments M_S at 10 K and resistivity values at 250 K parallel/perpendicular to terraces.

Sample	$[SRO/STO]_n$	t_B (uc)	a (nm)	T_C (K)	M_S (μ_B/uc)	ρ ($\mu\Omega$ cm)
F2	$[2/0]_1$	—		(50)	—	36/32 685
F4	$[4/0]_1$	—		135	1.2	62/6395
F12	$[12/0]_1$	—		140	1.5	83/188
F100	$[100/0]_1$	—		150	1.9	212/120
SL3/3	$[3/3]_{15}$	5.9 ± 0.1	0.392 ± 0.0005	85	0.55	265/1020
SL6/9	$[6/9]_{15}$	14.0 ± 0.1	0.391 ± 0.0005	132	1.3	215/570
SL12/4	$[12/4]_{15}$	17.4 ± 0.1	0.392 ± 0.0005	142	1.6	140/305

and the appearance of induced ferromagnetic order in the antiferromagnetic $SrMnO_3$ layers [16, 17]. It is an open question, however, how large the induced moments (if any) at the $SrRuO_3/SrTiO_3$ are and whether the coupling between Ru and Ti moments is also antiferromagnetic as is the case of the Ru–O–Mn bond [17, 18].

In this work we have studied the structural, magnetic and transport properties of thin $SrRuO_3$ films as well as $SrRuO_3/SrTiO_3$ superlattices grown on $SrTiO_3$(001). The structural studies were focused on an exploration of the sharpness of the $SrRuO_3/SrTiO_3$ interface as a prerequisite for the observation of interfacial magnetic and transport effects. With magnetic and transport measurements we tried to elucidate the emergence of an interfacial ferromagnetic state.

2. Experimental details

$SrRuO_3$(SRO) films and $SrRuO_3/SrTiO_3$ superlattices (SLs) were fabricated by pulsed laser deposition from stoichiometric polycrystalline targets. Vicinal $SrTiO_3$ (STO) (001) substrates with a small miscut angle of about 0.1°, uniform TiO_2-termination and a terrace morphology with typically 150–400 nm terrace width were used. The substrate was heated to 650 °C and the partial pressure of oxygen was 0.14 mbar. The samples studied in this work are listed in table 1 with respective layer thicknesses. Samples are either denoted by the film thickness or by the individual layer thicknesses, both specified by the number of unit cells (uc) of the pseudocubic lattice.

The microstructure of the SLs was investigated by high angle annular dark field-scanning transmission electron microscopy (HAADF-STEM) in a TITAN 80–300 FEI microscope; energy dispersive x-ray spectroscopy (EDX) was performed, in order to probe the atomic structure of the interfaces and to check for chemical intermixing. TEM measurements were carried out in a transmission electron microscope of type CM20T (Philips) working with a primary electron energy of 200 keV. AFM measurements were made with a Veeco DI5000, x-ray diffractometry was made with a Philips X'Pert system; the bilayer thickness t_b and the average lattice constant a of the superlattices were determined from an analysis of the superlattice reflections and are listed in table 1. Resistance and Hall effect measurements were made with a standard four-point probe technique in van der Pauw configuration. The longitudinal and Hall resistivity were calculated taking into account the thickness of the conducting SRO layers only.

Magnetization measurements were performed in a SQUID magnetometer. After subtraction of the diamagnetic magnetization contribution all samples showed a ferromagnetic hysteresis loop, even above the Curie temperature of $SrRuO_3$. This is consistent with magnetization measurements on a range of substrates as reported in [19]. This ferromagnetic contribution, measured at 200 K, was subtracted from all hysteresis loops. We did not attempt, however, to correct for the paramagnetic contribution of the $SrTiO_3$ substrate, since the substrate-to-substrate variations were too large [19]. In general the concentration of paramagnetic impurities in $SrTiO_3$ was small and the paramagnetic upturn at low temperatures was negligible for all samples except for the 2 unit cell thick SRO film F2.

3. Results

3.1. Structural characterization

Figure 1 shows θ–2θ scans of the superlattices around the (001) reflection of the STO substrates. For all superlattices satellite reflections at least up to the second order were seen. From the position of the satellite peaks the bilayer thickness t_B was determined as listed in table 1. These values are in good agreement with layer thicknesses as determined from the deposition time and verified by TEM analysis.

All samples were characterized by AFM measurements. Figure 2 shows selected AFM scans of SLs SL12/4 and SL3/3 as well as the single film F4. The superlattices showed step-flow growth with the vicinal terraces of the STO substrate clearly to be seen on the sample surface. On the SLs SL12/4 and SL3/3 adjacent terraces were separated by unit cell high steps. The thin films, however, have a different morphology. Although one-dimensional features running along the substrate's terraces show up on the film surface, these are not of unit cell height. As shown in figure 2(d) these features are better described as trenches. Films F4 and F2 with thicknesses of about 1.6 and 0.8 nm have trenches with typical depths of about 1 and 0.5 nm. This means that the trenches do not reach the substrate surface and that the films are continuous. However, they have some tendency towards one-dimensional structures with wire widths of about 200 (F4) and 160 nm (F2). One might therefore expect an in-plane anisotropy in both transport and

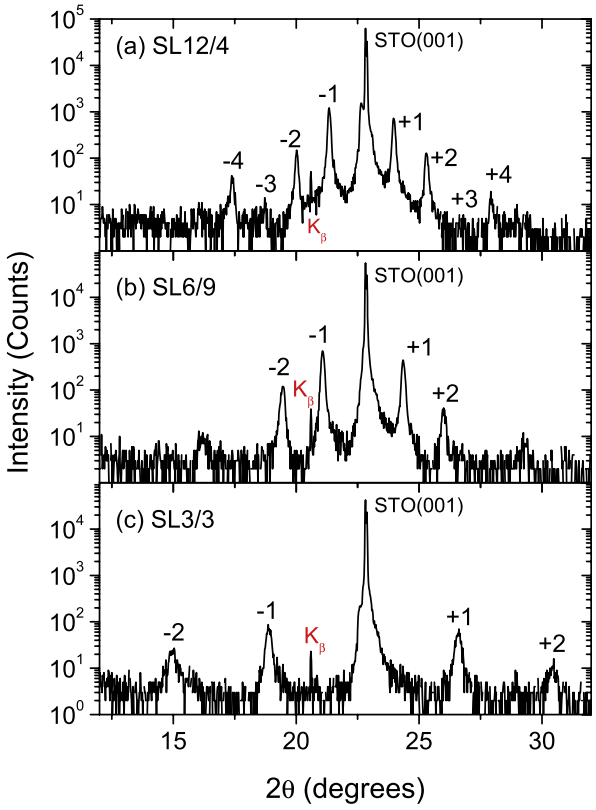

Figure 1. θ–2θ scans near the (001) reflection of the $SrTiO_3$ substrate for superlattices (a) SL12/4, (b) SL6/9 and (c) SL3/3. Satellite reflections are indexed; the K_β line is also indicated.

magnetic properties, as will be discussed in later sections. The formation of the linear structures was attributed to a segregation of SrO and TiO_2 terminations on the $SrTiO_3$ surface [20]. Along the step edges of the TiO_2 terminated terraces, half-cell deep SrO terminated trenches are formed. Since the SRO wetting behaviour differs for the two surface terminations, the films grow preferentially on the terraces leaving trenches at the step edges [20].

A plan-view TEM image of film F12 as well as larger scale HAADF-STEM images of the superlattices SL12/4 and SL3/3 are shown in figure 3. The plan-view image in figure 3(a) clearly shows the substrate terraces as a regular array of nearly vertical lines. The orthorhombic *c*-axis $[001]_o$ is parallel to the terraces. Moreover, in this image area of about 135 μm^2 three defects are visible as dark spots (close to the bottom right corner, near the left rim and above the '3'), i.e. defects occur in this film, but they are rare. Further TEM images of SRO thin films can be found in [21]. The HAADF-STEM images of the superlattices SL12/4 and SL3/3 in figures 3(b) and (c) show a regular layer structure on length scales of 100 and 25 nm, respectively. In SL3/3 a substrate deformation is seen close to the interface with the first SRO layer that propagates into the superlattice, but is then healed out. These overview images convey the impression that defects are comparatively rare in the samples.

High resolution HAADF-STEM micrographs of the SLs SL3/3 and SL12/4 are shown in figure 4. The interfaces between the SRO and STO layers were coherent, see also comparable $La_{0.7}Sr_{0.3}MnO_3$ /SRO superlattices [22–24]. The cations could be identified from the HAADF-STEM contrast such that the SRO and STO layers could be assigned; in figure 4(a) some ionic positions are indicated. Sometimes Ru and Ti columns cannot be easily distinguished, indicating some degree of Ru/Ti intermixing. From the EDX maps and line scans in figure 4, it is evident that down to a layer thickness of 2 unit cells the layers retain a clear $SrRuO_3$

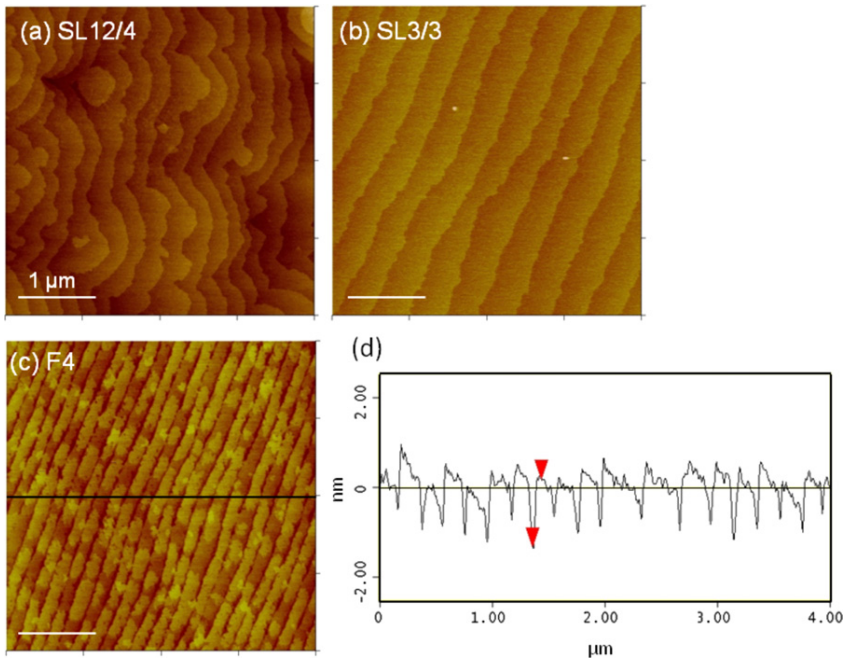

Figure 2. AFM images of samples (a) SL12/4, (b) SL3/3 and (c) F4. Scan size is 4 μm × 4 μm. In (d) a cross-section scan for film F4 along the black line is shown.

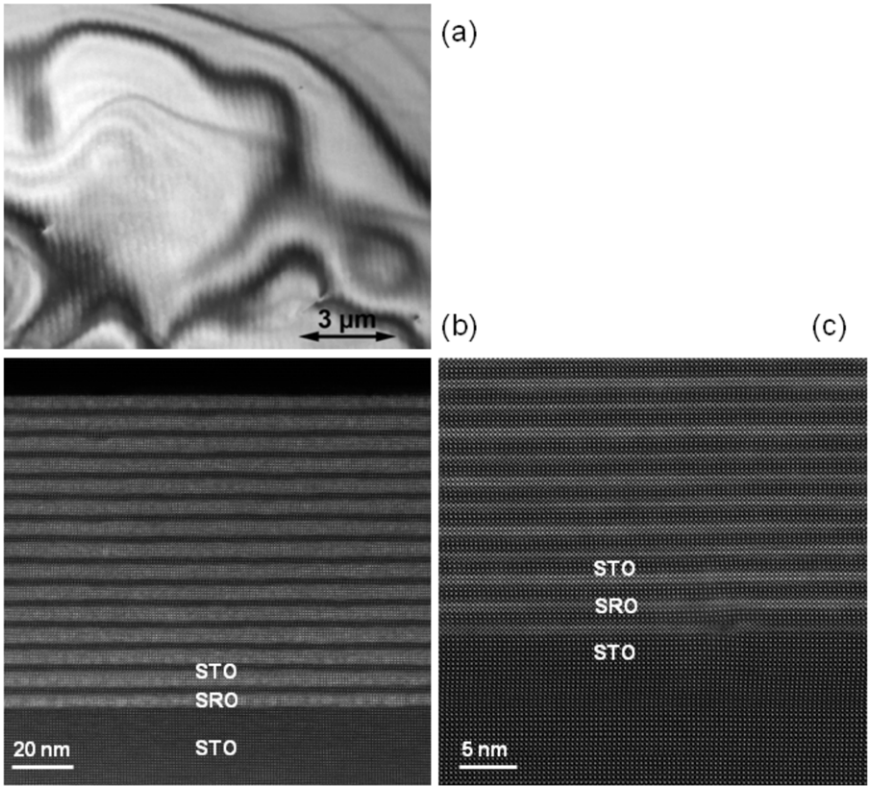

Figure 3. TEM and HAADF-STEM overview images. (a) Plan-view TEM image of SRO film F12. The regular array of vertical stripes is due to the terraces on the substrate. The long and thick, dark bowed lines are bending contours of the thin sample. (b) Larger scale HAADF-STEM image of superlattice SL12/4 showing homogeneous layering of SRO (brighter) and STO (darker) layers. (c) Larger scale HAADF-STEM image of superlattice SL3/3 with substrate defect close to the interface between STO substrate and first SRO layer.

or $SrTiO_3$ character. There might, however, be some Ru/Ti intermixing on a length scale of about 0.6 nm, including a possible small beam broadening, as can be seen in the EDX line scan in figure 4(b). This intermixing might influence the existence of interfacial magnetic states and especially the formation of an electron gas at the SRO/STO interface. Indeed, in the case of the $La_{0.7}Sr_{0.3}MnO_3$/SRO interface, Ru/Mn intermixing leads to a strong suppression of the Ru magnetic moment [18]. Furthermore, interface roughness leads to a suppression of the Mn magnetic moment in $LaMnO_3/SrMnO_3$ superlattices, whereas sharp interfaces lead to an enhanced interfacial Mn magnetic moment [25, 26]. To our knowledge, there are no studies of the influence of intermixing on the magnetic properties of SRO/STO interfaces; note, however, that the present experimental interfaces are not identical to the sharp interfaces considered theoretically [10, 11] and might affect the magnetic behaviour.

3.2. Magnetic properties

The magnetic moment versus temperature curves of superlattice SL3/3 and thin films F4 and F2 are shown in figure 5. Measurements were made in an applied field of 0.1 T on field cooling (FCC) from 200 K and in remanence (REM) after removing the applied field at 5 K. The 4 unit cell thick film has a rather high Curie temperature of about 135 K and a bulk-like temperature dependence of the magnetic moment. There is a large anisotropy between the [110] and [001] directions, with the latter clearly being a hard axis. Since the field cooled and remanent magnetization nearly agree along the [110] direction, one might conclude that the surface normal is close to the easy axis as also found in thicker SRO films [21, 27]. The magnetic moment versus temperature curves for the superlattice SL3/3 are rather similar, albeit with a much more gradual temperature dependence. The magnetocrystalline anisotropy of this sample is the same as that of the 4 unit cell thick film. The crystalline symmetry of the samples will be further discussed in sections 3.3.2 and 3.3.3. Here we just want to point out that all of the SRO layers have orthorhombic symmetry—except for superlattice SL3/3 which has tetragonal symmetry. The possible orientations of the orthogonal and tetragonal cells with respect to the cubic STO cell are shown in figure 5 (right). The $[110]_o$ direction of the orthorhombic cell is along the $[001]_c$ direction of the STO substrate [28], whereas the $[001]_t$ direction of the tetragonal cell is along the $[001]_c$ direction of the STO substrate [29]. Accordingly, the magnetization data of SL3/3 in figures 5(a) and 6(a) are indexed within a tetragonal cell, whereas the corresponding data for the thin film F4 are indexed within an orthorhombic cell.

The 2 unit cell thick SRO film F2 shown in figure 5(c) has a very weak signal due to the smaller volume, but also due to the weakening of the ferromagnetic order, and it is difficult to separate this signal from the substrate signal. Therefore

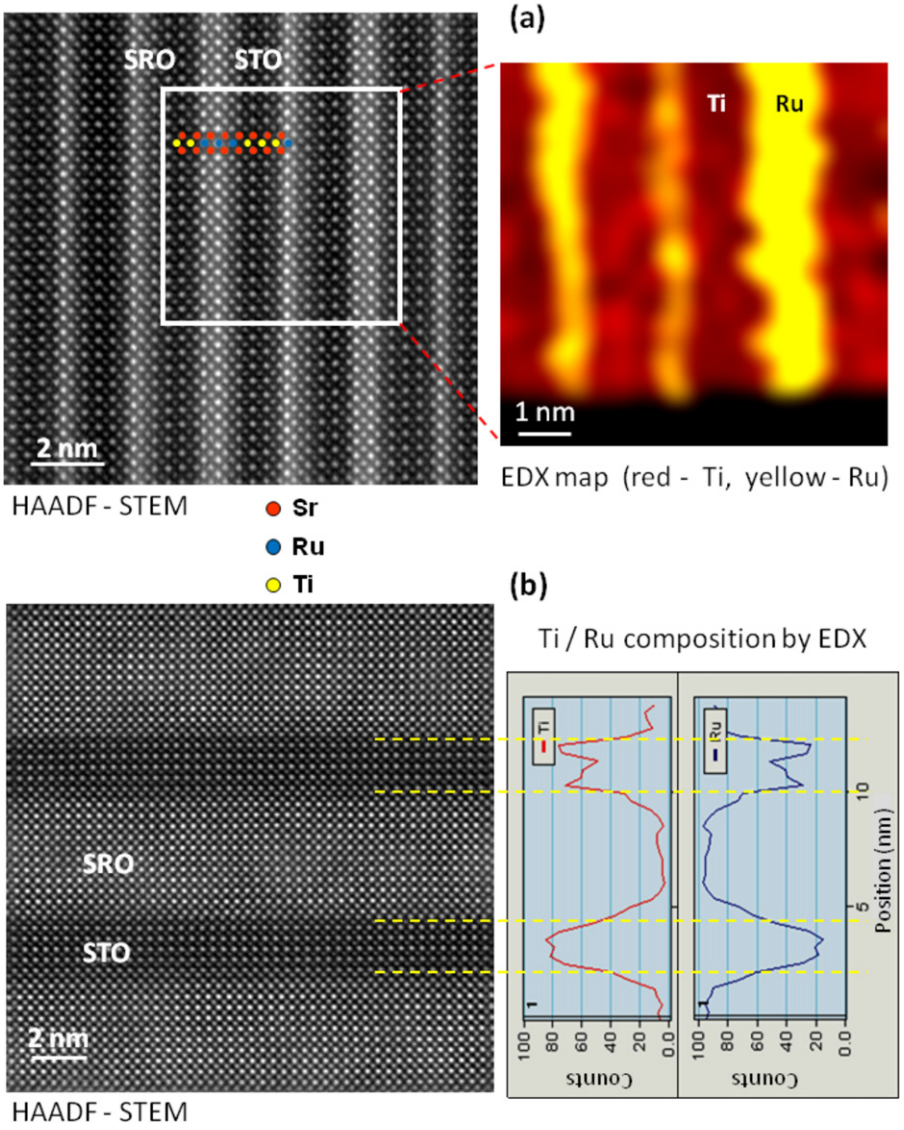

Figure 4. (a) HAADF-STEM image of SL3/3 (left) and corresponding EDX map (right). (b) HAADF-STEM image of SL12/4 with corresponding Ti and Ru EDX line scans along the growth direction.

only the remanent magnetization is shown in figure 5(c). The in-plane remanent magnetization shows an upturn below 50 K indicating some ferromagnetic order at low temperatures. In contrast to film F4, the magnetocrystalline anisotropy is modified by the thickness reduction, with the easy axis moving from the out-of-plane direction for the 4 unit cell to an in-plane direction for the 2 unit cell thick film.

The magnetic moment versus magnetic field curves of SRO film F4 and superlattice SL3/3 are shown in figures 6(a) and (b). At 10 K both samples have a rather large coercivity, 1.75 T for sample F4 and 0.75 T for sample SL3/3, in agreement with the large magnetocrystalline anisotropy of SRO [21, 30–32]. The saturation magnetic moments of both samples are considerably reduced with respect to the bulk magnetic moment of 1.6 μ_B/Ru [33]. This might be attributed to a reduced Ru magnetic moment at the SRO/STO interface. Such a reduction might be understood within two scenarios: in the first, the magnetic moment is quenched just by the presence of the interface, in the second, as suggested by Xia *et al* [13], the Ru spins at the interface order antiferromagnetically. It is impossible to determine from our global magnetization measurements which scenario holds, since both effectively remove the contribution of the interfacial Ru magnetic moments to the measured magnetization. In the case of superlattice SL12/4 this would amount to a reduction of the average magnetic moment to a value of 10/12 of the bulk moment and in the case of SL3/3 even to a value of 1/3 of the bulk magnetic moment. If we regard the magnetic moment of 1.9 μ_B measured for the 40 nm thick film F100 as bulk value, than we would estimate magnetic moment values of 1.6, 1.3 and 0.6 μ_B for superlattices SL12/4, SL6/9 and SL3/3, just on the basis of these reduction factors. These values are in good agreement with the measured values for the superlattices, see table 1. In the case of the thin films, the measured magnetic moments are in a slightly worse agreement with this scenario; this indicates that also the SRO–vacuum interface is magnetically reconstructed; for oxygen controlled SRO

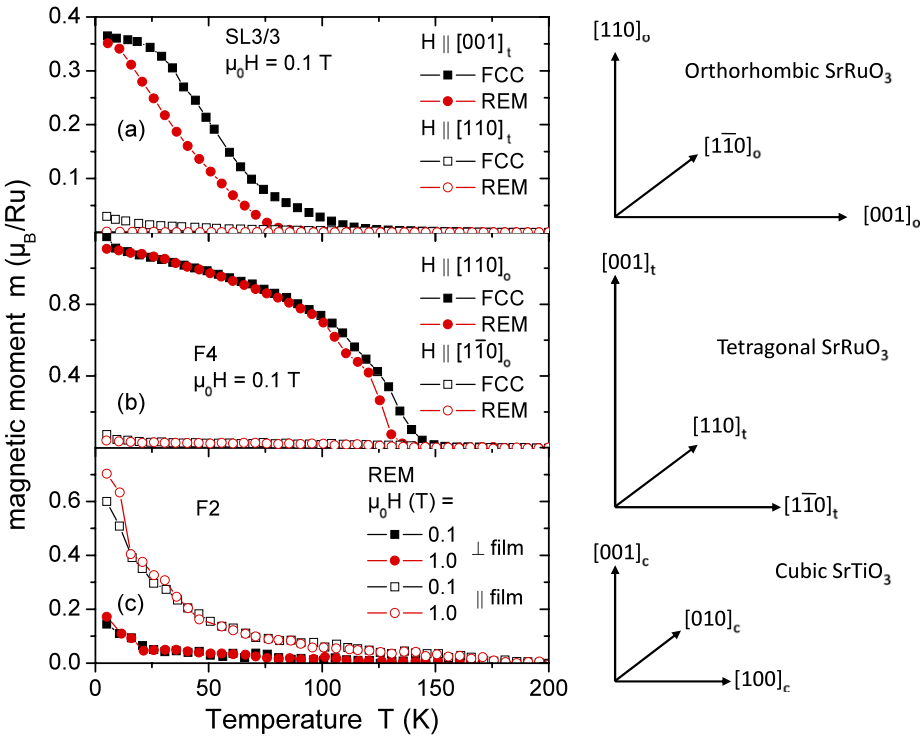

Figure 5. Left: magnetic moment versus temperature curves recorded on field cooling (FCC) and in the remanent state (REM) for samples (a) SL3/3 and (b) F4. The magnetic field of 0.1 T was applied either parallel (open symbols) or perpendicular (solid symbols) to the sample plane. (c) The remanent magnetization of film F2 measured after field cooling the film in applied fields of 0.1 and 1 T parallel and perpendicular to the film. The field was removed at 5 K. Right: relative orientation of the orthorhombic and tetragonal $SrRuO_3$ unit cells with respect to the cubic $SrTiO_3$(001) substrate.

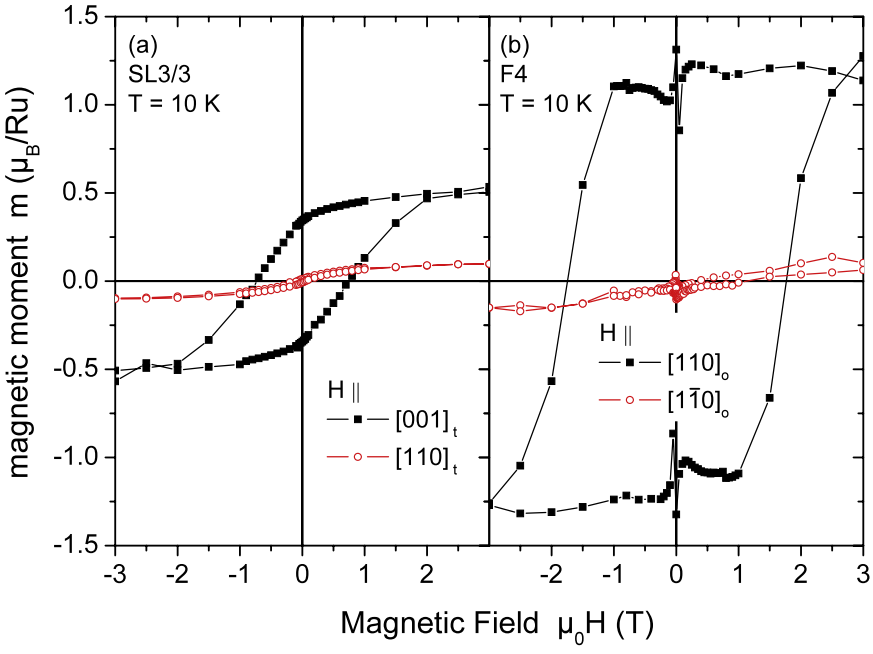

Figure 6. Magnetic moment versus magnetic field curves of (a) thin film F4 and (b) superlattice SL3/3 at 10 K.

surface reconstructions see also [34, 35]. The shape of the magnetization loops reported here is in good agreement with polar Kerr effect loops reported by Xia *et al* [13], but not with the hysteresis loops measured on 1 unit cell thick SRO/STO superlattices by Gu *et al* [12] which are more reminiscent of background hysteresis loops from the substrates [19]. The latter discrepancy may be related to a modified anisotropy for very small SRO layer thicknesses as observed in film F2.

Figure 7 shows the Curie temperature, the low temperature magnetic moment as well as the magnetization

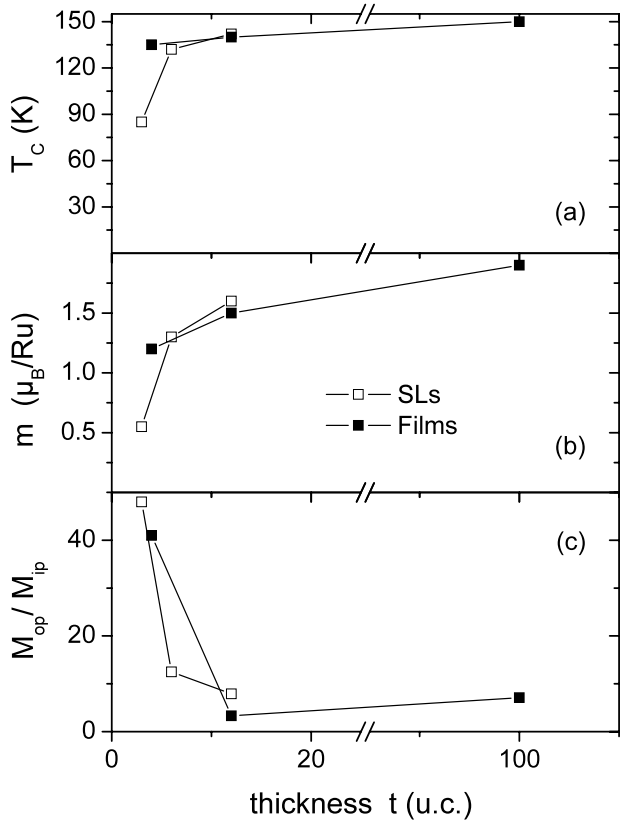

Figure 7. (a) Curie temperature, (b) saturation magnetic moment at 10 K and (c) magnetization ratio for magnetic fields applied out-of-plane (M_{op}) and in-plane along the magnetically hard axis (M_{ip}) as a function of SRO film or layer thickness.

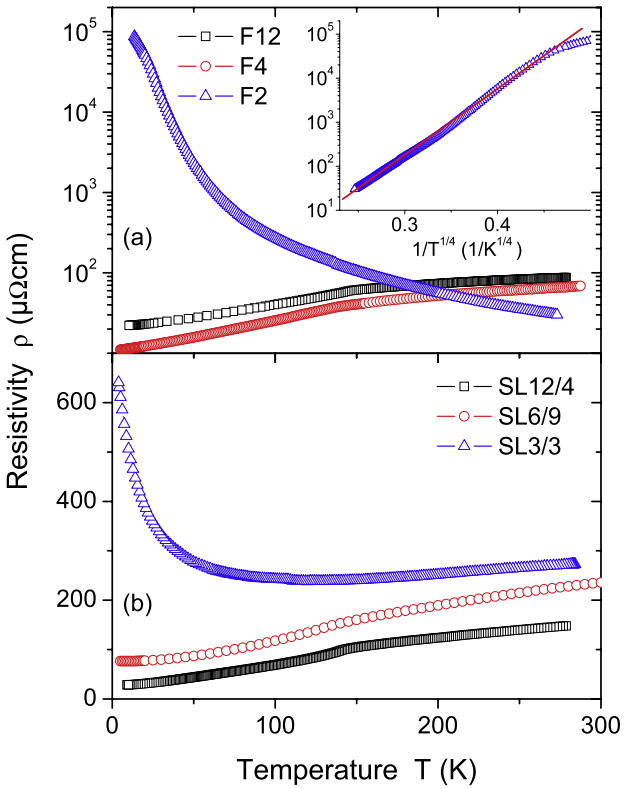

Figure 8. Resistivity of the $SrRuO_3$ (a) thin films and (b) superlattices as a function of temperature. The inset shows the resistivity of film F2 on a $\ln -1/T^{1/4}$ scale. The red line is a guide to the eye.

anisotropy between easy and hard axes, M_{op}/M_{ip}, as a function of film or layer thickness. The Curie temperature decreases with decreasing layer thickness as expected from finite size scaling [36, 37]. Similar trends were observed in SRO/STO superlattices [38] as well as in thin films [13, 39]. In view of the limited number of data points we did not attempt to determine the critical exponent. It is clear from figure 7(a) that a strong downturn in Curie temperature starts at a thickness of about 3 unit cells. The saturation magnetic moment shows the same trend as a function of layer thickness as the Curie temperature, see figure 7(b). Note that the 40 nm thick film has a saturation moment of 1.9 μ_B/Ru, considerably higher than the bulk magnetic moment of 1.6 μ_B/Ru [33]. Such an enhancement of the magnetic moment has been reported before by Grutter *et al* [40], where also magnetic moments up to 2 μ_B/Ru were observed in SRO films on STO (001); the enhancement is even higher in SRO films grown on STO (110) and (111) substrates [40]. The magnetic moment enhancement was attributed to the stabilization of a Ru^{4+} high-spin state by the substrate induced strain [41]. The anisotropy ratios of the magnetization shown in figure 7(c) were determined from measurements of the remanent magnetization as a function of temperature after field cooling in a field of 0.1 T. The anisotropy increase with reduced film thickness might be attributed to magnetostriction, see the discussion below.

3.3. Magnetotransport properties

3.3.1. Resistivity. The in-plane resistivity of the samples is anisotropic, see [21, 42] and the resistivity values in table 1. Partially, we attribute this anisotropy to the crystalline anisotropy with the resistivity being somewhat higher along the $[001]_o$ direction than along the $[1\bar{1}0]_o$ direction [21]. The main contribution to the resistivity anisotropy, however, is due to the growth anisotropy as discussed in section 3.1 and elsewhere [42]. Here we focus on a comparison of the resistivity of the films and superlattices; to this end the smaller resistivity value for each sample is shown as a function of temperature in figure 8. Both thin films and superlattices show the same trend: the resistivity of the SRO layers (films) changes from metallic to non-metallic below a thickness of about 4 unit cells. Whereas the room temperature resistivity of all samples is not very different, the resistivity of the 2 unit cell thick film increases by three orders of magnitude on cooling down to 10 K. This film follows a variable-range hopping law between 20 and 300 K, see inset to figure 8. The overall resistivity phenomenology of these samples is in good agreement with the results reported in [13] and is similar to the behaviour of $SrRuO_3$ layers in superlattices with $LaAlO_3$ [43].

3.3.2. Magnetoresistance. The magnetoresistance of the 4 and 2 unit cell thick films as well as superlattice

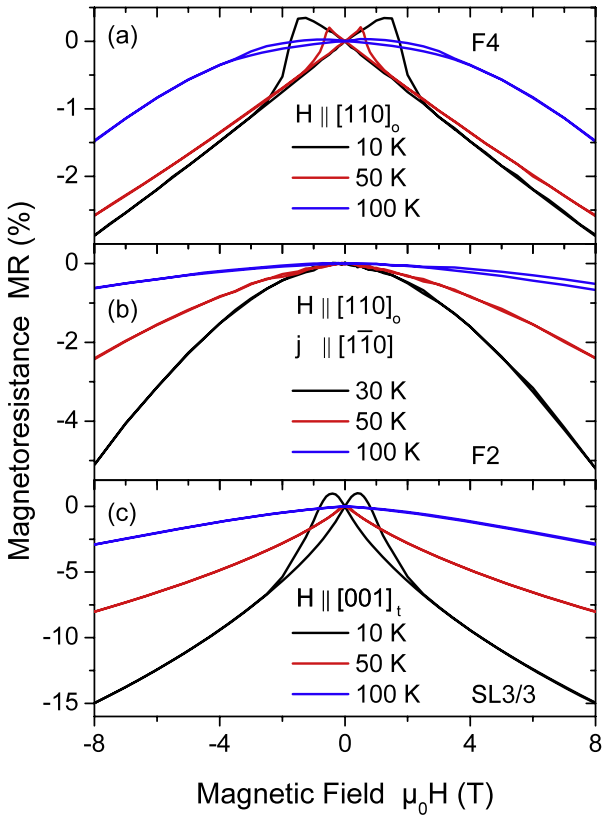

Figure 9. Magnetoresistance of $SrRuO_3$ (a) film F4, (b) film F2 and (c) superlattice SL3/3 as a function of magnetic field at various temperatures. The magnetic field was applied perpendicular to the samples along either $[110]_o$ or $[001]_t$, the current density was along $[1\bar{1}0]$.

SL3/3 is shown in figure 9. The magnetic field was applied perpendicular to the sample plane, the current was in-plane along the $[1\bar{1}0]_o$ resp. $[1\bar{1}0]_t$ direction. The magnetoresistance hysteresis at low temperatures shows the typical butterfly loop characteristic of ferromagnets. Therefore we identify the magnetoresistance mechanism as anisotropic magnetoresistance [44]; this is consistent with the comparatively large values of the resistivity, see figure 8, which preclude the observation of Lorentz magnetoresistance. In agreement with the measured values of the Curie temperature, see table 1, magnetic hysteresis is seen in the magnetoresistance of film F4 at 10, 50 and 100 K and of superlattice SL3/3 at 10 and 50 K (the latter hysteresis seen only after magnification). The magnetoresistance of film F2 is, within measurement uncertainty, non-hysteretic at temperatures of 30 K and above; the curve shape, however, is not fully parabolic, therefore it is not possible to exclude ferromagnetic order in this film. At 8 T and low temperatures the magnetoresistance of the superlattice SL3/3 is much larger than that of the thin film F4. Although this might be related to the change in crystalline symmetry from orthorhombic to tetragonal, one has to stress that the absolute value of the magnetoresistance strongly depends on the value of the residual resistivity and the transport processes contributing to the latter. Since the magnetoresistance observed in tetragonal SRO thin films was rather small [45], a correlation between the size of the magnetoresistance and the crystalline symmetry cannot be confirmed.

Figure 10 shows the angular magnetoresistance of superlattice SL3/3 in a magnetic field of 8 T. The latter was rotated within the $(110)_t$ and $(\bar{1}10)_t$ planes; in both cases the current was applied along the $[110]_t$ and $[\bar{1}10]_t$ directions. Measurements were done between 10 and 100 K. The magnetoresistance curves evolved continuously between the 10 and 100 K curves shown in figure 10. Following the analysis in [21, 29], one might infer the crystalline symmetry of the superlattice from the symmetry of the magnetoresistance. The most striking feature of the data is the similarity of the magnetoresistance curves for rotation around the $[110]_t$ and $[\bar{1}10]_t$ planes; this similarity is not perfect, but not expected for an orthorhombic unit cell with the $[001]_o$ axis being along one of the in-plane directions. Further the curves do not show much resemblance to the typical angular magnetoresistance data of orthorhombic $SrRuO_3$ films or layers [21, 29, 46]. Therefore we indexed the sample with a tetragonal unit cell with the $[001]_t$ direction along the surface normal and the $[110]_t$ and $[\bar{1}10]_t$ directions along the substrate [100] and [010] directions. This indexing is further discussed in the section about the Hall effect.

We do not wish to embark on an extensive fitting of the magnetoresistance data. We note that the magnetoresistance curves at 10 K have a cusp at 90°, i.e. when the magnetic field is rotated through the superlattice plane. This indicates that a magnetic hard axis is located along these directions. Indeed, this feature of the magnetoresistance curves might be understood within a model of magnetization rotation in a ferromagnet with uniaxial anisotropy energy

$$E_K = K_u \sin^2\Theta \tag{1}$$

with θ being the angle between the magnetization vector and the surface normal and $K_u > 0$ denoting the uniaxial magnetocrystalline constant. Taking the Zeeman energy into account, the total energy is given by

$$E = E_K - \mu_0 \vec{H} \cdot \vec{M}_S \tag{2}$$

with the saturation magnetization $\vec{M}_S$; μ_0 denotes the vacuum permittivity. The latter equation was minimized with respect to the magnetization angle at a given angle Θ_F between the magnetic field and the surface normal. For the magnetoresistance an angle dependence proportional to $\cos^2\Theta$ was used. This yields the solid red lines shown in figure 10. These capture the behaviour of the magnetoresistance for angles close to the superlattice plane quite well. The only parameter within this model is the anisotropy field $\mu_0 H_A = 2K_u/M_S$ which is obtained as 6 T at 10 K and 1 T at 100 K for superlattice SL3/3. The corresponding angular magnetoresistance curves of film F4 are similar to the angular magnetoresistance of the superlattice and are not shown here. Fitting the model to the magnetoresistance of film F4 yielded anisotropy fields of $\mu_0 H_A = 6$ T at 100 K and 1.3 T at 150 K; these are considerably larger than the values of superlattice SL3/3.

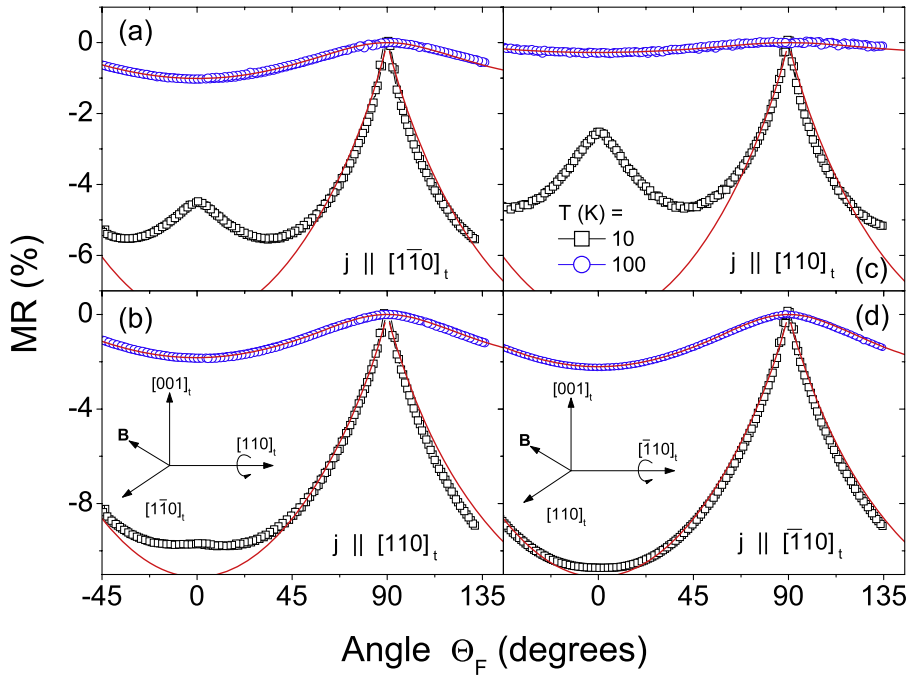

Figure 10. Magnetoresistance of $SrRuO_3$ superlattice SL3/3 for magnetic field rotations in the (a), (b) $(110)_t$ and (c), (d) $(\bar{1}10)_t$ planes. Current density was along either the $[110]_t$ or the $[1\bar{1}0]_t$ direction. Magnetic field was 8 T, measurement temperatures 10 and 100 K. The insets indicate the axis orientations. The solid lines were calculated from the model discussed in the text.

The strong increase of the magnetic anisotropy might be related to magnetostriction. If the SRO films or layers are regarded to be pseudocubic with a lattice constant $a_{SRO} = 0.393$ nm, then the enhancement of the anisotropy field due to magnetostriction is given by [47]

$$\Delta H_A = \frac{3\lambda_{100}}{\mu_0 M_S}(c_{11} - c_{12})\left(1 + \frac{2c_{11}}{c_{12}}\right)\epsilon \qquad (3)$$

with the magnetostriction coefficient λ_{100}, the saturation magnetization $\mu_0 M_S \simeq 0.3$ T, the elastic moduli [48] $c_{11} = 252$ GPa and $c_{12} = 132$ GPa and the strain ϵ. In the case of the 4 unit cell thick film at 100 K we might estimate $\mu_0 \Delta H_A = 6$ T. Under the assumption that this film is fully strained, $\epsilon = (a_{SRO} - a_{STO})/a_{SRO} = 0.006$, the magnetostriction coefficient is estimated as $\lambda_{100} = 1.4 \times 10^{-4}$. This value is somewhat smaller than the magnetostriction estimated by Dabrowski *et al* [49], but is about a factor of 3–4 larger than λ_{100} of the manganites [47].

3.3.3. Hall effect. The Hall resistivity ρ_{yx} of SRO films F4 and F2 as well as superlattices SL6/9 and SL3/3 had an anomalous contribution, related to the magnetization at low magnetic fields, before crossing over to a contribution linear in applied field that we identify as the ordinary Hall effect, see also [42]:

$$\rho_{yx} = \mu_0(R_H H + R_A M), \qquad (4)$$

where M denotes the magnetization component perpendicular to the sample plane and R_H and R_A are the ordinary and anomalous Hall coefficients. For all samples the high field slope is negative, i.e. electron conduction prevails as is known for $SrRuO_3$ [33, 50–52]. The anomalous Hall constant of samples F4, F2 and SL6/9 is negative in agreement with measurements on orthorhombic SRO films [45, 52–55]. The anomalous Hall constant of superlattice SL3/3, however, is positive. Since the sign of the anomalous Hall effect depends sensitively on the crystalline symmetry [45, 46, 56, 57], this is clear evidence that the SRO layers in superlattice SL3/3 have tetragonal symmetry. This is consistent with the conclusion from the angular magnetoresistance measurements discussed above. Since the SRO film F2 shows an anomalous Hall effect at 50 K, we might further conclude that this film is ferromagnetic at low temperatures; we could not, however, determine the Curie temperature of this film. It was already shown in [42] that the Hall resistivity ρ_{yx} versus magnetic field curves of the thicker superlattices neatly follow equation (4), when the measured magnetization is used for M. In superlattice SL3/3, however, there are significant deviations between the field dependence of the Hall resistivity and the measured magnetization [42]. This has been also observed in $Pr_{0.7}Ca_{0.3}MnO_3/SrRuO_3$ superlattices [56], and might be attributed to the magnetic interlayer coupling.

The anomalous Hall constant $\rho_{yx,A}$ was determined by extrapolation of the ordinary Hall effect to zero field. The corresponding values for $\rho_{yx,A}$ are presented in figure 11(a) for the films and superlattices. Although there is some sample-to-sample variation, the anomalous Hall contribution of the samples with orthorhombic SRO layers follows the typical temperature dependence, being negative at low temperatures and turning positive somewhere between 100 and 150 K [45, 51, 52, 58–60]. At higher temperatures $\rho_{xy,A} = \mu_0 R_A M$ vanishes, since the extrapolated value of the magnetization vanishes above the Curie temperature [61]. In contrast, the

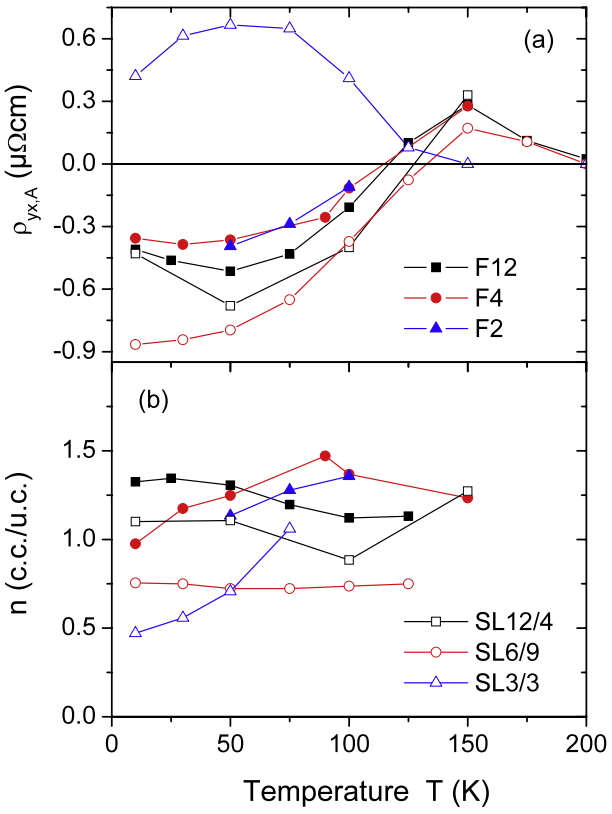

Figure 11. (a) Anomalous Hall effect $\rho_{yx,A}$ and (b) carrier concentration per unit cell as a function of temperature.

anomalous Hall contribution of superlattice SL3/3 is positive throughout the measured temperature range in agreement with the results on a tetragonal SRO film [45]. The carrier density as calculated from a one band model, $n = -1/(eR_H)$, is shown in figure 11(b) as a function of temperature. Deep within the ferromagnetic phase the carrier density is temperature independent within experimental uncertainty in the range—with some sample-to-sample variation—of 1 ± 0.5 electrons per unit cell. This value is consistent with literature values [56, 62].

4. Discussion and conclusions

In this work a thorough study of the structural, magnetic, magnetoresistance and Hall effect properties of $SrRuO_3$ films and $SrRuO_3/SrTiO_3$ superlattices was presented. This study was driven by the theoretical prediction of the emergence of a spin-polarized electron gas at the SRO/STO interface [10, 11]. The growth conditions of SRO on STO had been optimized [63] and HAADF-STEM images showed coherent interfaces. However, a certain degree of Ru/Ti intermixing on a length scale of 1–1.5 unit cells could not be excluded. The crystalline symmetry of the SRO layers was indirectly inferred from angle dependent magnetoresistance measurements as well as from the sign of the anomalous Hall effect. Both techniques indicate that the SRO films as well as superlattices with thicker SRO layers had orthorhombic symmetry; the superlattice SL3/3 with layers of three pseudocubic unit cells each, however, had tetragonal symmetry. This might be related to an odd/even effect: multiples of a $[110]_o$ oriented SRO orthorhombic cell do fit in two or four pseudocubic layers, but not in three.

In single films ferromagnetic order was verified by magnetization measurements and the presence of the anomalous Hall effect down to a film thickness of 2 unit cells. In the case of the superlattices, clear ferromagnetic order with a Curie temperature of 85 K was found for $SrRuO_3$ layers with a thickness of 3 unit cells. Compared to thick SRO films the thin SRO layers show three differences in their magnetic properties: (1) the Curie temperature and (2) the average magnetic moment per Ru ion strongly decrease below a layer thickness of about 4 unit cells; (3) the magnetocrystalline anisotropy strongly increases with the out-of-plane direction being magnetically easy. The first observation is related to a finite size effect and the latter to magnetostriction; both effects are common in thin magnetic films. The decrease of the magnetic moment can be very well explained by assuming non-ferromagnetic interfacial SRO layers of unit cell thickness. This indicates the absence of a spin-polarized interfacial electron gas. The latter conclusion is confirmed by the absence of any signatures of interfacial conduction. In contrast, resistivity measurements showed a crossover from metallic to insulating behaviour on reduction of the $SrRuO_3$ layer thickness with a critical thicknesses of 3 unit cells.

In conclusion, the samples do not show a ferromagnetic interfacial state. Whether this is related to the observed Ru/Ti intermixing or is intrinsic to the SRO/STO interface has to be clarified by further studies.

Acknowledgments

This work was supported by the DFG within SFB 762 ‘Functionality of Oxide Interfaces’; FB is member of the Leipzig School of Natural Sciences ‘BuildMoNa’. We thank P Esquinazi for a critical reading of the manuscript.

References

[1] Reyren N *et al* 2007 *Science* **317** 1196
[2] Brinkman A, Huijben M, van Zalk M, Huijben J, Zeitler U, Maan J C, van der Wiel W G, Rijnders G, Blank D H A and Hilgenkamp H 2007 *Nature Mater.* **6** 493
[3] Ariando *et al* 2011 *Nature Commun.* **2** 288
[4] Dikin D A, Mehta M, Bark C W, Folkman C M, Eom C B and Chandrasekhar V 2011 *Phys. Rev. Lett.* **107** 056802
[5] Li L, Richter C, Mannhart J and Ashoori R C 2011 *Nature Phys.* **7** 762
[6] Bert J A, Kalisky B, Bell C, Kim M, Hikita Y, Hwang H Y and Moler K A 2011 *Nature Phys.* **7** 767
[7] Okamoto S, Millis A J and Spaldin N A 2006 *Phys. Rev. Lett.* **97** 056802
[8] Pentcheva R and Pickett W E 2007 *Phys. Rev. Lett.* **99** 016802
[9] Chambers S A *et al* 2010 *Surf. Sci. Rep.* **65** 317
[10] Verissimo-Alves M, García-Fernández P, Bilc D I, Ghosez P and Junquera J 2012 *Phys. Rev. Lett.* **108** 107003
[11] García-Fernández P, Verissimo-Alves M, Bilc D I, Ghosez P and Junquera J 2012 *Phys. Rev.* B **86** 085305
[12] Gu M, Xie Q, Shen X, Xie R, Wang J, Tang G, Wu D, Zhang G P and Wu X S 2012 *Phys. Rev. Lett.* **109** 157003

[13] Xia J, Siemons W, Koster G, Beasley M R and Kapitulnik A 2009 *Phys. Rev.* B **79** 140407
[14] Padhan P and Prellier W 2005 *Phys. Rev.* B **72** 104416
[15] Padhan P and Prellier W 2006 *Appl. Phys. Lett.* **88** 263114
[16] Choi Y, Yoo Y Z, Chmaissem O, Ullah A, Kolesnik S, Kimball C W, Haskel D, Jiang J S and Bader S D 2007 *Appl. Phys. Lett.* **91** 022503
[17] Choi Y, Tseng Y C, Haskel D, Brown D E, Danaher D and Chmaissem O 2008 *Appl. Phys. Lett.* **93** 192509
[18] Ziese M *et al* 2010 *Phys. Rev. Lett.* **104** 167203
[19] Khalid M, Setzer A, Ziese M, Esquinazi P, Spemann D, Pöppl A and Goering E 2010 *Phys. Rev.* B **81** 214414
[20] Bachelet R, Sánchez F, Santiso J, Munuera C, Ocal C and Fontcuberta J 2009 *Chem. Mater.* **21** 2494
[21] Ziese M, Vrejoiu I and Hesse D 2010 *Phys. Rev.* B **81** 184418
[22] Ziese M, Vrejoiu I and Hesse D 2010 *Appl. Phys. Lett.* **97** 052504
[23] Ziese M, Vrejoiu I, Pippel E, Nikulina E and Hesse D 2011 *Appl. Phys. Lett.* **98** 132504
[24] Hillebrand R, Pippel E, Hesse D and Vrejoiu I 2011 *Phys. Status Solidi* a **208** 2144
[25] May S J, Shah A B, te Velthuis S G E, Fitzsimmons M R, Zuo J M, Zhai X, Eckstein J N, Bader S D and Bhattacharya A 2008 *Phys. Rev.* B **77** 174409
[26] Shah A B, Ramasse Q M, May S J, Kavich J, Wen J G, Zhai X, Eckstein J N, Freeland J, Bhattacharya A and Zuo J M 2010 *Phys. Rev.* B **82** 115112
[27] Kolesnik S, Yoo Y Z, Chmaissem O, Dabrowski B, Maxwell T, Kimball C W and Genis A P 2006 *J. Appl. Phys.* **99** 08F501
[28] Gan Q, Rao R A, Eom C B, Wu L and Tsui F 1999 *J. Appl. Phys.* **85** 5297
[29] Ziese M, Vrejoiu I, Pippel E, Hähnel A, Nikulina E and Hesse D 2011 *J. Phys. D: Appl. Phys.* **44** 345001
[30] Landau L, Reiner J W and Klein L 2012 *J. Appl. Phys.* **111** 07B901
[31] Kanbayasi A 1976 *J. Phys. Soc. Japan* **41** 1879
[32] Kanbayasi A 1978 *J. Phys. Soc. Japan* **44** 89
[33] Cao G, McCall S, Shepard M, Crow J E and Guertin R P 1997 *Phys. Rev.* B **56** 321
[34] Shin J, Borisevich A Y, Meunier V, Zhou J, Plummer E W, Kalinin S V and Baddorf A P 2010 *ACS Nano* **4** 4190
[35] Tselev A, Ganesh P, Qiao L, Siemons W, Gai Z, Biegalski M D, Baddorf A P and Kalinin S V 2013 *ACS Nano* **7** 4403
[36] Schneider C M, Bressler P, Schuster P, Kirschner J, de Miguel J J and Miranda R 1990 *Phys. Rev. Lett.* **64** 1059
[37] Farle M, Baberschke K, Stetter U, Aspelmeier A and Gerhardter F 1993 *Phys. Rev.* B **47** 11571
[38] Izumi M, Nakazawa K and Bando Y 1998 *J. Phys. Soc. Japan* **67** 651
[39] Chang Y J, Kim C H, Phark S H, Kim Y S, Yu J and Noh T W 2009 *Phys. Rev. Lett.* **103** 057201
[40] Grutter A, Wong F, Arenholz E, Liberati M, Vailionis A and Suzuki Y 2010 *Appl. Phys. Lett.* **96** 082509
[41] Grutter A J, Wong F J, Arenholz E, Vailionis A and Suzuki Y 2012 *Phys. Rev.* B **85** 134429
[42] Bern F and Ziese M 2013 *EPJ Web Conf.* **40** 15013
[43] Liu Z Q *et al* 2012 *Appl. Phys. Lett.* **101** 223105
[44] Gunnarsson R 2012 *Phys. Rev.* B **85** 235409
[45] Bern F, Ziese M, Dörr K, Herklotz A and Vrejoiu I 2013 *Phys. Status Solidi RRL* **7** 204
[46] Kan D, Aso R, Kurata H and Shimakawa Y 2013 *Adv. Funct. Mater.* **23** 1129
[47] Ziese M, Semmelhack H and Busch P 2002 *J. Magn. Magn. Mater.* **246** 327
[48] Yamanaka S, Maekawa T, Muta H, Matsuda T, Kobayashi S and Kurosaki K 2004 *J. Solid State Chem.* **177** 3484
[49] Dabrowski B, Avdeev M, Chmaissem O, Kolesnik S, Klamut P W, Maxwell M and Jorgensen J D 2005 *Phys. Rev.* B **71** 104411
[50] Allen P B, Berger H, Chauvet O, Forro L, Jarlborg T, Junod A, Revaz B and Santi G 1996 *Phys. Rev.* B **53** 4393
[51] Klein L, Reiner J R, Geballe T H, Beasley M R and Kapitulnik A 2000 *Physica* B **281/282** 608
[52] Kats Y, Genish I, Klein L, Reiner J W and Beasley M R 2004 *Phys. Rev.* B **70** 180407
[53] Mathieu R, Asamitsu A, Yamada H, Takahashi K S, Kawasaki M, Fang Z, Nagaosa N and Tokura Y 2004 *Phys. Rev. Lett.* **93** 016602
[54] Mathieu R, Jung C U, Yamada H, Asamitsu A, Kawasaki M and Tokura Y 2005 *Phys. Rev.* B **72** 064436
[55] Koster G, Klein L, Siemons W, Rijnders G, Dodge J S, Eom C B, Blank D H A and Beasley M R 2012 *Rev. Mod. Phys.* **84** 253
[56] Ziese M and Vrejoiu I 2011 *Phys. Rev.* B **84** 104413
[57] Fang Z, Nagaosa N, Takahashi K S, Asamitsu A, Mathieu R, Ogasawara T, Yamada H, Kawasaki M, Tokura Y and Terakura K 2003 *Science* **302** 92
[58] Klein L, Reiner J R, Geballe T H, Beasley M R and Kapitulnik A 2000 *Phys. Rev.* B **61** R7842
[59] Khalifah P, Ohkubo I, Sales B C, Christen H M, Mandrus D and Cerne J 2007 *Phys. Rev.* B **76** 054404
[60] Haham N, Shperber Y, Schultz M, Naftalis N, Shimshoni E, Reiner J W and Klein L 2011 *Phys. Rev.* B **84** 174439
[61] Haham N, Reiner J W and Klein L 2012 *Phys. Rev.* B **86** 144414
[62] Kobayashi Y, Iwata M, Kaneko T, Sato K, Asai K and Ohsumi H 2010 *Phys. Rev.* B **82** 174430
[63] Vrejoiu I, Alexe M, Hesse D and Gösele U 2008 *Adv. Funct. Mater.* **18** 3892